Open access • Journal Article • DOI:10.1088/0004-637X/815/2/95

The VMC Survey. XVIII. Radial Dependence of the Low-mass, 0.55--0.82 M Stellar Mass Function in the Galactic Globular Cluster 47 Tucanae — Source link

C. Zhang, C. Zhang, Chengyuan Li, Chengyuan Li ...+16 more authors

Institutions: Chinese Academy of Sciences, Peking University, Purple Mountain Observatory, International Space Science Institute ...+7 more institutions

Published on: 14 Dec 2015 - The Astrophysical Journal (IOP Publishing)

Topics: Globular cluster, Star cluster, Stellar mass, Galaxy and Galaxy cluster

The Astrophysical Journal, 815:95 (9pp), 2015 December 20 doi:10.1088/0004-637X/815/2/95

THE VMC SURVEY. XVIII. RADIAL DEPENDENCE OF THE LOW-MASS, 0.55–0.82 $M_{\odot}$ STELLAR MASS FUNCTION IN THE GALACTIC GLOBULAR CLUSTER 47 TUCANAE

Chaoli Zhang[1,2], Chengyuan Li[1,3,4], Richard de Grijs[1,3,5], Kenji Bekki[6], Licai Deng[7], Simone Zaggia[8], Stefano Rubele[8], Andrés E. Piatti[9,10], Maria-Rosa L. Cioni[11,12,13], Jim Emerson[14], Bi-Qing For[7], Vincenzo Ripepi[15], Marcella Marconi[15], Valentin D. Ivanov[16], and Li Chen[2]

[1] Kavli Institute for Astronomy & Astrophysics, Peking University, Yi He Yuan Lu 5, Hai Dian District, Beijing 100871, China; jackzcl@outlook.com, grijs@pku.edu.cn
[2] Shanghai Astronomical Observatory, Chinese Academy of Sciences, Shanghai 200030, China
[3] Department of Astronomy, Peking University, Yi He Yuan Lu 5, Hai Dian District, Beijing 100871, China
[4] Purple Mountain Observatory, Chinese Academy of Sciences, Beijing Xi Lu, Nanjing 210008, China
[5] International Space Science Institute-Beijing, 1 Nanertiao, Zhongguancun, Hai Dian District, Beijing 100190, China
[6] ICRAR M468, The University of Western Australia, 35 Stirling Highway, Crawley, WA, 6009, Australia
[7] Key Laboratory for Optical Astronomy, National Astronomical Observatories, Chinese Academy of Sciences, 20A Datun Road, Chaoyang District, Beijing 100012, China
[8] INAF-Osservatorio Astronomico di Padova, vicolo dell'Osservatorio 5, I-35122 Padova, Italy
[9] Observatorio Astrońomico, Universidad Nacional de Córdoba, Laprida 854, 5000, Córdoba, Argentina
[10] Consejo Nacional de Investigaciones Científicas y Técnicas, Av. Rivadavia 1917, C1033AAJ, Buenos Aires, Argentina
[11] Universität Potsdam, Institut für Physik und Astronomie, Karl-Liebknecht-Str. 24/25, D-14476 Potsdam, Germany
[12] Leibnitz-Institut für Astrophysik Potsdam, An der Sternwarte 16, D-14482 Potsdam, Germany
[13] Physics, Astronomy, and Mathematics, University of Hertfordshire, Hatfield AL10 9AB, UK
[14] Astronomy Unit, School of Physics and Astronomy, Queen Mary University of London, Mile End Road, London E1 4NS, UK
[15] INAF-Osservatorio Astronomico di Capodimonte, via Moiariello 16, I-80131 Naples, Italy
[16] European Southern Observatory, Karl-Schwarzschild-Str. 2, Garching bei München, D-85748, Germany
Received 2015 August 25; accepted 2015 November 4; published 2015 December 14

ABSTRACT

We use near-infrared observations obtained as part of the *Visible and Infrared Survey Telescope for Astronomy* (VISTA) Survey of the Magellanic Clouds (VMC), as well as two complementary *Hubble Space Telescope* (*HST*) data sets, to study the luminosity and mass functions (MFs) as a function of clustercentric radius of the main-sequence stars in the Galactic globular cluster 47 Tucanae. The *HST* observations indicate a relative deficit in the numbers of faint stars in the central region of the cluster compared with its periphery, for $18.75 \leqslant m_{\rm F606W} \leqslant 20.9$ mag (corresponding to a stellar mass range of $0.55 < m_{*}/M_{\odot} < 0.73$). The stellar number counts at 6.′7 from the cluster core show a deficit for $17.62 \leqslant m_{\rm F606W} \leqslant 19.7$ mag (i.e., $0.65 < m_{*}/M_{\odot} < 0.82$), which is consistent with expectations from mass segregation. The VMC-based stellar MFs exhibit power-law shapes for masses in the range $0.55 < m_{*}/M_{\odot} < 0.82$. These power laws are characterized by an almost constant slope, α. The radial distribution of the power-law slopes α thus shows evidence of the importance of both mass segregation and tidal stripping, for both the first- and second-generation stars in 47 Tuc.

Key words: galaxies: clusters: individual (47 Tucanae) – globular clusters: general – Hertzsprung–Russell and C–M diagrams – stars: low-mass – stars: luminosity function, mass function

1. INTRODUCTION

The globular clusters (GCs) in the Milky Way are excellent probes to study the Galaxy's formation history. One of the major goals in contemporary astrophysics is to understand the stellar mass functions (MFs) of GCs, because they are thought to contain original information about the stellar initial mass function (IMF). A number of physical processes can cause the IMF to vary, including fragmentation, accretion, feedback, stellar interactions, and magnetic-field contributions (Larson 1992; Padoan & Nordlund 2002; Bonnell et al. 2007). A detailed understanding of the IMF is required to study the stellar populations of external galaxies, which would otherwise be impossible to study owing to their unresolved nature.

However, it is not simple to derive the IMF from an observed present-day MF, since the latter is affected by both observational and theoretical limitations: observationally, it is significantly impaired by the crowding of GCs, photometric uncertainties, and the observational field of view, which can lead to significant biases when attempting to determine the underlying stellar luminosity function (LF; King 1958). The situation is further complicated by the fact that the mass–luminosity relation (MLR), which is required to transform the observed stellar luminosities to the corresponding masses, is metallicity- and age-dependent (e.g., Kroupa et al. 1990; de Grijs et al. 2002). Theoretical MLRs for intermediate and high stellar masses ($m_{*} \geqslant 0.2M_{\odot}$) are relatively well constrained observationally, but at the low-mass end ($m_{*} \leqslant 0.2M_{\odot}$) significant uncertainties remain. In addition, the MF can also be modified by dynamical processes over a cluster's lifetime. For instance, tidal interactions with the Milky Way's gravitational potential affect the outskirts of clusters (Lane et al. 2012), while mass segregation affects their central regions (e.g., de Grijs et al. 2002).

Despite all these observational and theoretical challenges, the MF of the Galactic GC 47 Tucanae (47 Tuc) has been studied extensively. Paust et al. (2010) showed that the 47 Tuc MF in the cluster's central region can be approximated by a power-law distribution, i.e., $dN/dM \propto M^{-\alpha}$, with $\alpha = 0.84$ for the stellar mass range of 0.2–0.8$M_{\odot}$; de Marchi & Paresce (1995) and Santiago et al. (1996) showed that the MF at a location between 4′ and 5′ from the center (close to the cluster's

half-mass radius) is a power law with $\alpha = 1.5$ for the mass range of 0.3–0.8 $M_{\odot}$, but that it flattens in the range 0.14–0.3 $M_{\odot}$. Comparison with the most recent Monte Carlo simulations by Giersz & Heggie (2011) showed that the stars above the main-sequence (MS) turn-off in 47 Tuc obey a power law with $\alpha = 2.8$ and follow a relatively flat IMF with an index of about 0.4 along the lower MS. This mass distribution is much shallower than that found based on the ground-based observations of Hesser et al. (1987), who determined an index of 1.2 for the mass range of 0.5–0.8 $M_{\odot}$. However, all stellar MFs investigated in previous studies pertained to specific loci in the cluster; some were located in the cluster center, some were based on data from its periphery, and some were determined around the half-mass radius. Here we present a systematic analysis covering a much larger radial range using ground-based data obtained with the 4 m *Visible and Infrared Survey Telescope for Astronomy* (VISTA) telescope as part of the VISTA Survey of the Magellanic Clouds (VMC), combined with *HST* observations at central and intermediate cluster radii, to investigate the low-mass MS LF and MF as a function of radius from the center of 47 Tuc.

This paper is organized as follows. In Section 2, we present the observational data and our analysis method. Our results are presented in Section 3. In Section 4, we discuss our results in the context of mass segregation and tidal stripping processes affecting 47 Tuc. Our conclusions are provided in Section 5.

2. DATA SELECTION AND ANALYSIS

2.1. VISTA Data

The near-infrared Y, J, and K_s observations used in this study were obtained as part of the VMC survey (Cioni et al. 2011). 47 Tuc is projected onto the Small Magellanic Cloud (SMC) and is located on VMC tile SMC 5_2. The SMC's main body is partially located on the adjacent, southern tile SMC 4_2. The VMC data were processed with the VISTA Data Flow System pipeline (VDFS) and calibrated to match the VISTA photometric system, which is close to the Vegamag system (Irwin et al. 2004). We extracted the paw-print VMC images for all three filters from the VISTA Science Archive and used the IRAF/DAOPHOT package to derive the point-spread functions (PSFs; Stetson 1987). The data selected for this study, composed of two epochs in the Y and J bands and nine in K_s, were PSF-homogenized and stacked to obtain a final, deep tile image.[17] We performed PSF photometry on the homogenized, deep VMC SMC 5_2 and 4_2 tiles image using the PSF and ALLSTAR tasks. The photometry was calibrated using the method described in Rubele et al. (2015). Subsequently, we correlated the three-band photometry to produce a multi-band catalog. Figure 1 shows the spatial distribution of the MS stars in 47 Tuc. The observations cover an area of almost 2×5 deg^2 (one VISTA InfraRed Camera—VIRCam—tile consists of six offset paw-print exposures covering a $\sim$1.6 deg^2 field of view), which contains more than 190,000 stars with $Y \in [16.8, 19.6]$ mag. A detailed overview of our observations of 47 Tuc as well as of our analysis procedures, was given by Li et al. (2014).

[17] We found that the VMC observations of 47 Tuc are significantly affected by PSF and sensitivity inhomogeneities for some epochs. For this reason, we selected only epochs characterized by minimal seeing variations and the highest sensitivity for analysis in the present paper, resulting in two epochs in the Y band, two and one concatenation in J (corresponding to two and a half epochs), and nine in K_s.

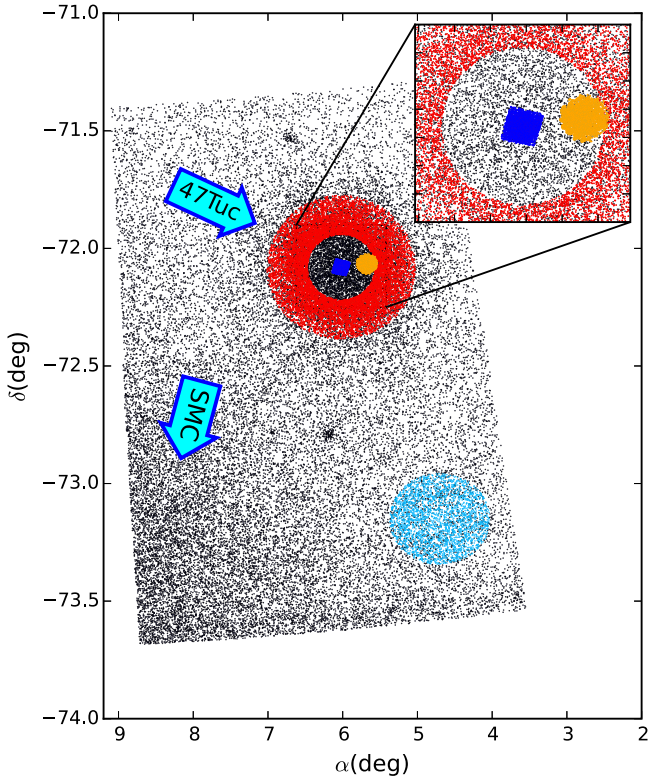

Figure 1. Spatial distribution of the stars in 47 Tuc (coordinates are given for the J2000 epoch), combining SMC tiles 5_2 (top half) and 4_2 (bottom half). The background stars were drawn from the VISTA data; the red annulus indicates the VMC data used for this study, which is further radially binned into five subsets. The blue region corresponds to the *HST* catalog of Sarajedini et al. (2007), and the orange region represents the ultra-deep *HST* catalog of Kalirai et al. (2012). The cyan region is adopted to compute the background field-star density, which is in turn used to decontaminate the cluster CMD.

The cluster is located toward the southwest in the SMC 5_2 tile image, while the southeastern corner of the field is dominated by SMC field stars. Therefore, the area occupied by 47 Tuc could contain significant numbers of field stars associated with both the SMC and the Milky Way. SMC tile 5_2 cannot be used for the field-star decontamination, since the cluster's tidal radius can reach $r_t = 2500''$ (Harris 1996; Lane et al. 2012), which essentially covers the entire tile. For background star decontamination, it is crucial to find a region that is representative both in terms of the star counts from the Milky Way and their counterparts from the variable SMC background. The bottom right-hand corner of the field, shown in cyan in Figure 1 and contained in SMC tile 4_2, is ideal for our decontamination of the cluster's color–magnitude diagram (CMD) from background stars, for two reasons. First, it is located at the same Galactic latitude as 47 Tuc so that Galactic field contamination should be similar to that affecting our 47 Tuc observations; second, this region is located at a suitable distance from both 47 Tuc and the SMC, thus minimizing the number of possible residual 47 Tuc and SMC stars.

We therefore adopted a region dominated by the 47 Tuc member stars centered at $\alpha_{J2000} = 00^h24^m04^s.80 (6^\circ.020)$, $\delta_{J2000} = -72^\circ04'48'' (-72^\circ.080)$ and within a radius of $1100''$ (Li et al. 2014). A second region, shown in cyan in Figure 1, centered on $\alpha_{J2000} = 00^h18^m48^s.00 (4^\circ.70)$, $\delta_{J2000} = -73^\circ09'02''(-73^\circ.15)$ with a radius of $600''$, was adopted to calculate the background stellar density.

Li et al. (2014) showed, for the same VMC data, that the observational completeness levels drop off rapidly in the cluster's inner region. This is caused by a combination of the increased blending probability and the enhanced background brightness. They performed a large number of artificial-star tests to study the effects of crowding on the uncertainties in the resulting PSF photometry. For details of the artificial-star tests, please refer to Rubele et al. (2012). The latter authors generated $\sim 10^6$ artificial stars in the image and repeated their PSF photometry in the same manner as for our sample of real stars. This resulted in an artificial-star catalog that contained the input and output magnitudes, as well as the photometric errors, computed as "output minus input" magnitudes. Our observations' completeness reaches a level of 50% at $Y = 19.6$ mag within a radius of 500″ from the cluster center. We therefore restricted our study to MS stars in an annulus defined by $r \in [500, 1100]''$ and $Y \in [16.8, 19.6]$ mag.

2.2. Hubble Space Telescope (HST) Data

We also made use of two different *HST* data sets of 47 Tuc to study the cluster's central regions, $r \in [0, 500]''$, which are not resolved by the VMC data. Both data sets were obtained with *HST*'s Advanced Camera for Surveys (ACS). One of the data sets was taken as part of the Globular Cluster Treasury program (PI: A. Sarajedini; Sarajedini et al. 2007, hereafter SA07), which aimed at obtaining accurate photometry for stars well below the MS turn-off in the F606W and F814W filters. We directly use the Anderson et al. (2008) catalog: see the blue data points in Figure 1.

Second, we used observations obtained by (Kalirai et al. 2012, hereafter KA12), who collected photometry for white dwarfs in 47 Tuc based on 121 orbits of Cycle 17 *HST* observations. Their main goal was to obtain photometry in the ACS F606W and F814W filters with extremely long exposure times to reach very faint magnitudes (approaching 29 mag in F606W) to study the entirety of the white dwarf cooling sequence in the cluster. The advantages of using the KA12 data are, first, that their field is located 6.′7 (8.8 pc) west of the cluster center. This region is neither too sparse nor too crowded for our analysis. It allows us to resolve large numbers of MS stars down to very low luminosities. Second, the authors' completeness tests demonstrate that their photometry is very precise and place the 50% completeness limit for the F606W filter at 29.75 mag. A detailed discussion of the observations and the corresponding data reduction can be found in KA12. The KA12 catalog data points are colored orange in Figure 1.

In the context of the study presented here, we emphasize that for both *HST* data sets, we restricted our study to magnitudes of $m_{\rm F606W} \in [17.53,20.9]$ mag for comparison with the VMC data. The *HST* data was decontaminated by proper-motion selection. This thus enabled us to construct highly robust local LFs.

2.3. Isochrone Fitting and MS Selection

A number of studies have demonstrated that 47 Tuc displays multiple stellar populations across its entire CMD (e.g., Anderson et al. 2009; Milone et al. 2012; Li et al. 2014). We therefore adopted slightly different isochrones to fit the CMDs corresponding to the different data sets used in this paper. Table 1 summarizes their basic parameters. The metallicity ([Fe/H]) adopted in the table decreases slightly (from [Fe/H] $= -0.66$ dex to [Fe/H] $= -0.82$ dex) with increasing radius, which is consistent with the results of Li et al. (2014), who found that stars in the cluster core are more metal-rich than their counterparts in the cluster's periphery. The theoretical isochrones we used to fit our CMDs were taken from the Dartmouth Stellar Evolution Program (DSEP; Dotter et al. 2008) for the *HST* data sets, since the DSEP models are highly commensurate with other models (e.g., Pietrinferni et al. 2006) and thus provide a robust and reliable MLR. However, the DSEP suite does not provide models in the VISTA Y, J, and K_s photometric system. Therefore, we adopted the Princeton–Goddard–Pontificia Universidad Católica (PGPUC[18]) stellar evolutionary code (Valcarce et al. 2012) to obtain best fits to the VMC data. The red curves in Figure 2 shows the CMDs and their corresponding best-fitting isochrones; the vertical purple lines in all panels show the magnitude ranges adopted for selecting the corresponding MS regime.

Table 1
Basic Representative 47 Tuc CMD Fit Parameters

Parameter	*HST* SA07	*HST* KA12	VISTA VMC
Model	DSEP[a]	DSEP	PGPUC[b]
t (Gyr)	12.5	12.5	12.5
Y	0.251	0.252	0.26
[Fe/H] (dex)	−0.66	−0.74	−0.83
[α/Fe] (dex)	0.0	0.4	0.3
$E(B-V)$ (mag)[c]	0.04	0.04	0.04
$(m-M)_0$ (mag)	13.3	13.3	13.35
$\alpha_{\rm J2000}$	$00^{\rm h}24^{\rm m}04\overset{\rm s}{.}80$	$00^{\rm h}22^{\rm m}39\overset{\rm s}{.}00$	…
$\delta_{\rm J2000}$	−72°04′48″	−72°04′04″	…
MS range (mag)	[17.53, 20.9]	[17.62, 20.9]	[16.8, 19.6]
Completeness (%)	[99, 85]	[100, 99.8]	[86, 65][d]

Note
[a] DSEP: Dotter et al. (2008).
[b] PGPUC: Valcarce et al. (2012).
[c] Harris (1996).
[d] For stars in an annulus with radii of 500″ and 1100″.

In order to select all MS stars in 47 Tuc with minimal contamination owing to photometric uncertainties, we characterized the photometric errors in each passband and each data set as follows. We first divided the magnitude range in each band into 100 bins and subsequently determined the mean photometric uncertainty in each bin. Subsequently, we interpolated the bin-averaged values. Figure 3 shows an example for the VISTA Y filter: the bin-averaged photometric uncertainties are plotted as the red curve, while the green curve represents the 5σ range. We also determined the fiducial ridge line of the MS stars in the CMDs, using bin sizes of 0.3 mag for $Y \in [16.8,\ 19.6]$ mag and $m_{F606W} \in [17.53,\ 20.9]$ mag. The fiducial ridge lines for all three data sets were then used to normalize the CMDs: see Figure 4. In this figure, the red curves indicate all stars selected within pre-determined photometric uncertainty ranges, i.e., 5σ, 4σ, and 5σ for SA07, KA12, and VMC data, respectively. This selection is required to limit unmodeled effects owing to the presence of a population of unresolved binary systems.

[18] http://www2.astro.puc.cl/pgpuc/iso.php

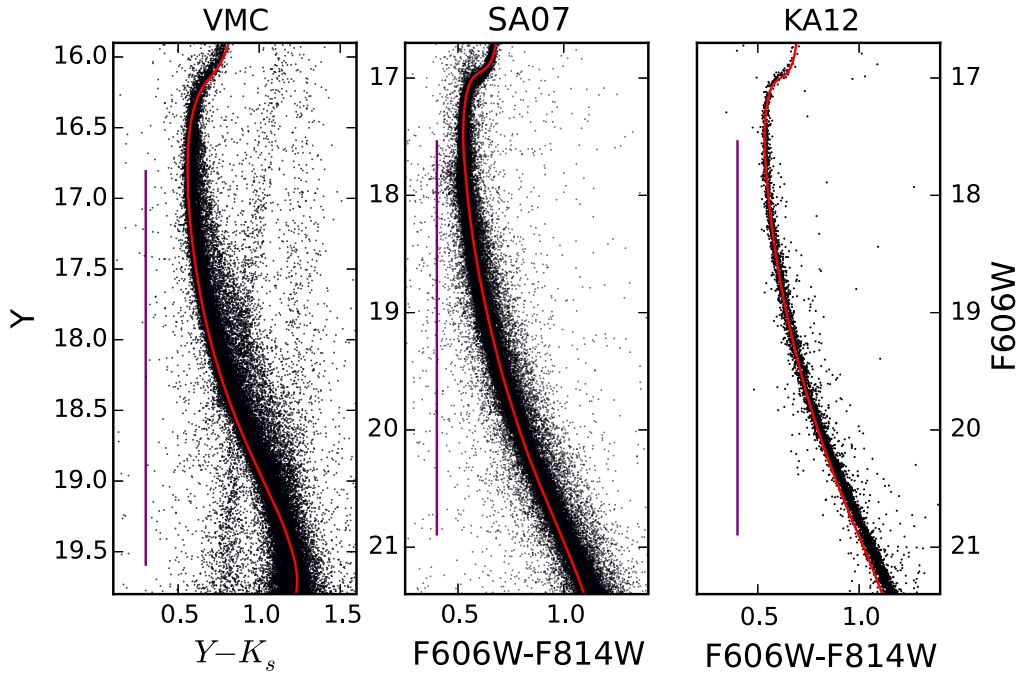

Figure 2. 47 Tuc CMDs. The red curves are the model isochrones defined in Table 1. The vertical purple lines indicate the magnitude ranges adopted for selecting MS stars.

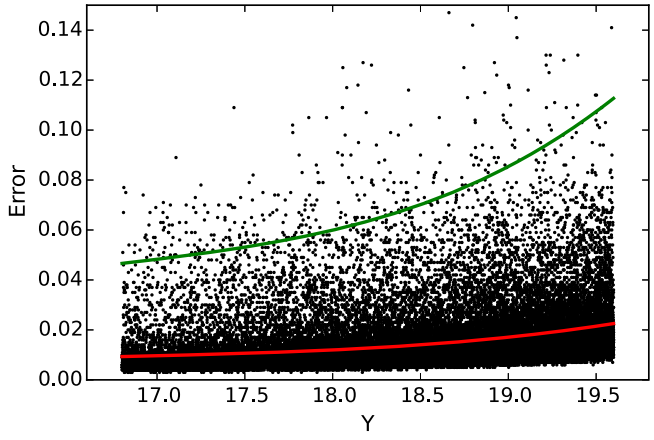

Figure 3. Photometric uncertainties as a function of magnitude for the VMC data set in the Y filter. The red solid curve represents the bin-averaged photometric uncertainties, while the green curve represents the 5σ range.

3. RESULTS

3.1. Luminosity Functions

The completeness-corrected local LFs based on the two *HST* data sets are shown in the top panel of Figure 5. The stars in both CMDs were divided into 15 bins. The error bars represent Poissonian counting statistics. The LFs extend over the magnitude range $17.53 \leqslant m_{\rm F606W} \leqslant 20.9$ mag. However, we note that the SA07 LF declines toward the low-mass end, for $18.75 \leqslant m_{\rm F606W} \leqslant 20.9$ mag, while the KA12 LF exhibits a deficit at the high-mass end, $17.62 \leqslant m_{\rm F606W} \leqslant 19.7$ mag. The vertical dashed lines in both panels indicate the decline on the left of the dashed line for SA07 and the deficit on the right for the KA12 data.

We consequently truncated the LF based on the SA07 data at the luminosity where the linear regime (indicated in green) is fitted adequately by a power law, i.e., $dN(L)/dL \propto L^{-\alpha}$, where $N(L)$ corresponds to the number of stars per unit luminosity L. To determine α statistically robustly, we ran Monte Carlo simulations, assuming that the stellar number counts in each bin are well-represented by Gaussian distributions. We then randomly drew stellar number counts from each bin to construct our sample LFs and fitted the results using a power law to obtain α. This random sampling based on Gaussian distributions in each bin was repeated ∼15,000 times. The resulting α distributions are shown in the right-hand panels of Figure 5, leading to (mean) $\mu_\alpha = 0.104$ for the SA07 data and $\mu_\alpha = 0.175$ for the KA12 catalog.

The VMC-based LF of 47 Tuc is shown at the bottom of Figure 5, also corrected for the effects of sampling incompleteness and field-star contamination. We divided the annulus $r \in [500, 1100]''$ further into five radial subsets, i.e., $r \in [500, 600]$, $r \in [600, 700]''$, $r \in [700, 800]''$, $r \in [800, 900]''$, and $r \in [900, 1100]''$. Applying the same routines as for the *HST* data, for each annulus we fitted the observed LFs with a power law and ran Monte Carlo simulations to obtain the distribution of α. The results showed that the LFs at different radii are all closely approximated by power laws, and that the α index increases toward the outer regions of the cluster.

3.2. Mass–luminosity Relation and MFs

To determine the stellar MF the observed LF is commonly divided by the derivative of the MLR. However, the shape of the MLR depends sensitively on the stellar model used. Figure 6 includes the three most-up-to-date stellar evolution models—DSEP (Dotter et al. 2008), PGPUC (Valcarce et al. 2012), and the Padova models (Marigo et al. 2008; Girardi et al. 2010)—in both the VISTA photometric system and for the *HST*/ACS photometric passbands used by SA07 and KA12. The stellar mass range we study here is $0.55 \leqslant m_*/M_\odot \leqslant 0.82$, a range where the input physics is relatively better constrained than at the low-mass end, and therefore all

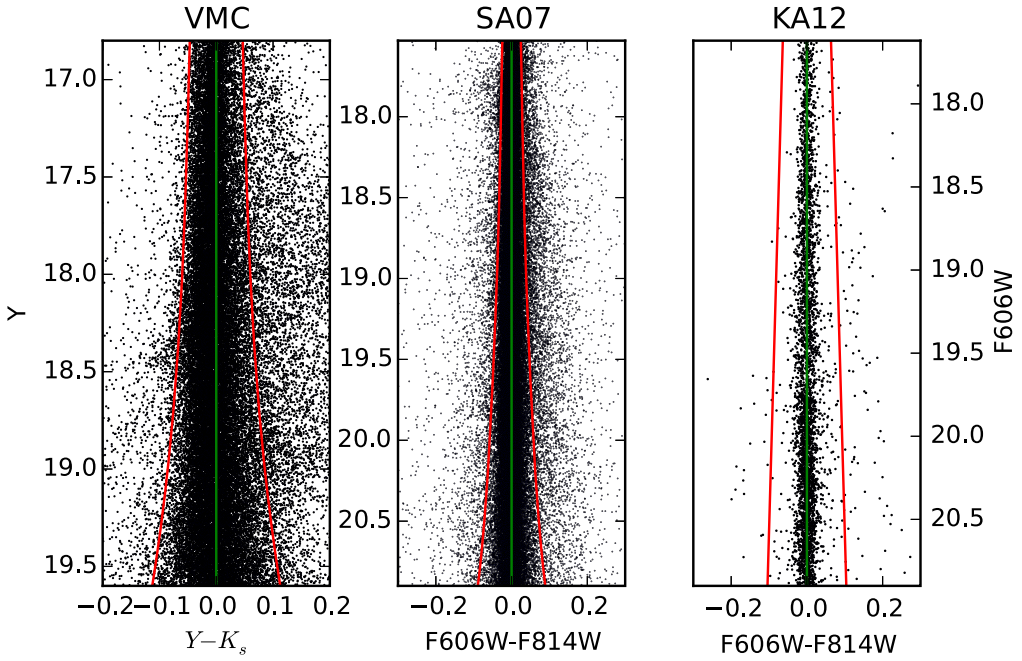

Figure 4. 47 Tuc CMD, "normalized" by removing the trend defined by the MS ridge line. The red lines are the 5σ, 4σ, and 5σ selections used to correct for the presence of background field stars. The green line is the zero-color reference.

models are characterized by smooth MLRs. We adopted PGPUC and DSEP as our reference models.

The left-hand panels of Figure 7 show the 47 Tuc MF for our two *HST* data sets and for the VMC data. The Monte Carlo simulation results for the α distribution of power-law fits are indicated in the right-hand panels. As already shown for the LFs, the SA07 MF shows a decline toward the low-mass end, for a mass range of $0.55 < m_*/M_\odot < 0.73$, whereas a deficit is again observed in the KA12 data for the high-mass end, at $0.65 < m_*/M_\odot < 0.82$ (see the red dashed lines). Similarly to our approach pertaining to the LFs, we truncated the SA07 MF where it starts to deviate from a power-law distribution and fitted a power law to this part of the MF. The resulting α distribution increases from $\alpha = 2.31$ (SA07; center) to $\alpha = 3.37$ (KA12; 6.′7 from the center), this result is in line with the expectations from mass segregation.

The local MFs based on our VMC data are shown at the bottom of Figure 7 for different clustercentric radii. The MFs are all power laws and exhibit almost constant α indices. The mean value of the five indices is $\langle\alpha\rangle = 3.13$, with a standard derivation of $\sigma_\alpha = 0.07$. We will discuss this flat trend in α index in the next section in the context of the effects of mass segregation and tidal stripping. For comparison, Bochanski et al. (2010) found $\alpha = 2.38$ for the MF of low-mass dwarfs in the field over the mass range $0.32\ M_\odot < m_* < 0.8\ M_\odot$, while Kalirai et al. (2013) determined that the field MF in the outer regions of the SMC for the stellar mass range $m_* \in [0.37, 0.93]\ M_\odot$ is well presented by a power-law with $\alpha = 1.9$. Except for the innermost annulus, our 47 Tuc MFs are thus steeper than expected for field stars, which reflects the effects of dynamical processing.

4. DISCUSSION

The observed MF α index increases from 2.31 in the central region (SA07) to 3.37 at intermediate radii (at $r \approx 6.'7$; KA12). This shows that mass segregation significantly affects the resulting stellar MF as a cluster undergoes dynamical relaxation (Anderson & King 1996). Dynamical mass segregation causes the high-mass stars to attain lower velocities, and they will thus gradually sink toward the cluster center and boost the lower-mass stars to the cluster's periphery. This will, in turn, lead to a flatter MF in the inner regions and a gradually steeper MF when moving toward the outskirts. This is evident for 47 Tuc, given the observed declining MF trend for low-mass stars in the central region, and the clear drop in stellar numbers starting from a mass of $m_* = 0.65 M_\odot$ or $\log(m_*/M_\odot) = -0.18$ dex. This drop cannot have been caused by incompleteness effects nor by field-star contamination, since the KA12 catalog is proper-motion cleaned and is 100% complete at the brightness levels of interest here. The radial diffusion of low-mass stars was recently observed for the first time by Heyl et al. (2015), based on a sample of young white dwarfs.

This dynamical evolution can be further complicated by the recent discovery that 47 Tuc hosts multiple stellar populations (Milone et al. 2012; Li et al. 2014). D'Ercole et al. (2010) and Bekki (2011) predicted that (i) the first-generation (FG) stars in a GC can be at least 5–10 times more massive that the second-generation (SG) stars at the epoch of GC formation and (ii) the SG population is much more centrally concentrated than their FG counterparts. This consequently leads to different two-body relaxation timescales ($t_{\rm relax}$) for the two populations, because $t_{\rm relax}$ depends on the GC mass and size for a given typical stellar mass. We emphasize that even though the observations indicate that approximately two-thirds of present-day cluster stars are SG descendants, with a substantial majority of FG stars having been stripped from their host clusters, it is still reasonable to discuss the effects of two-body relaxation on the dynamical evolution of a young 47 Tuc dominated by FG stars, because the stripping of FG stars takes hundreds of Myr. (Bekki 2011). We therefore investigated the half-mass relaxation timescales[19] $t_{\rm relax}$ *separately* for FG and SG stars to argue

[19] Here we use the median relaxation timescales (e.g., Spitzer & Hart 1971) just for convenience in the discussion.

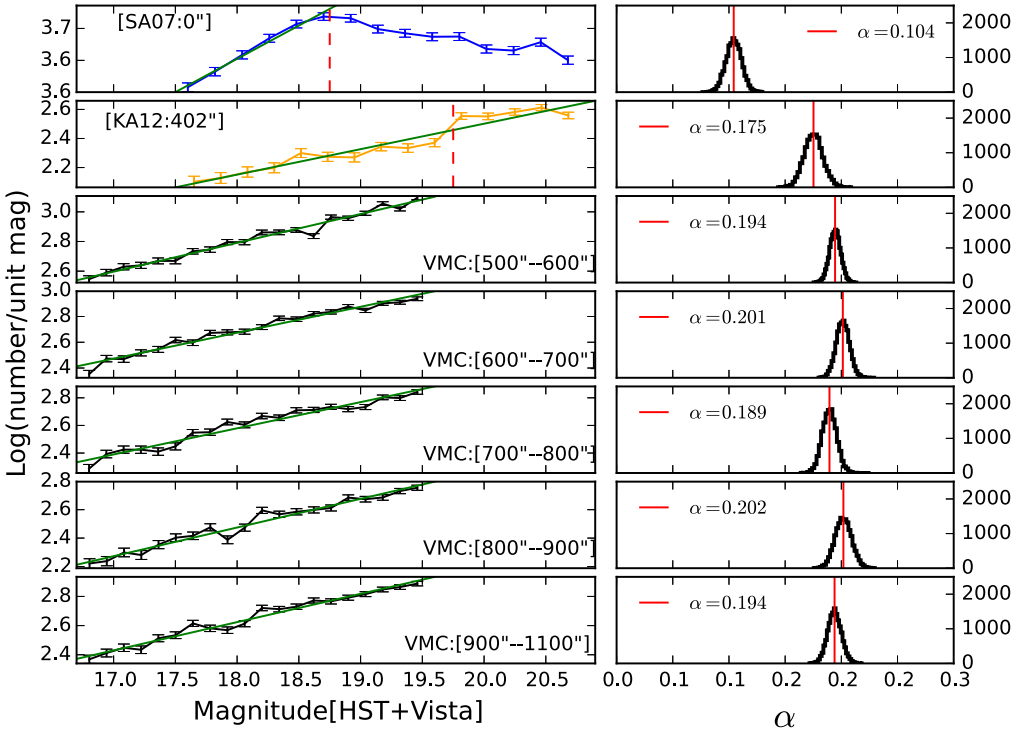

Figure 5. 47 Tuc MS LFs. LFs based on (top) the SA07 catalog for stars in the cluster center and (second panel) the KA12 catalog, containing stars located 6.′7 west of the cluster center. The bottom five panels are local LFs for radial annuli covered by our VMC observations. The full annulus, $r \in [500, 1100]''$, is divided into five radial subsets, i.e., $r \in [500, 600]''$, $r \in [600, 700]''$, $r \in [700, 800]''$, $r \in [800, 900]''$, and $r \in [900, 1100]''$. The numbers of MS stars per unit magnitude vs. apparent magnitude F606W are plotted; the error bars were estimated based on Poissonian counting statistics. The green line is the power-law fit to the LF, and the two arrows in top two panels are an indication of a possible LF break magnitude. The Gaussian distributions on the right are the results of our Monte Carlo simulations to determine the best-fitting power-law index α.

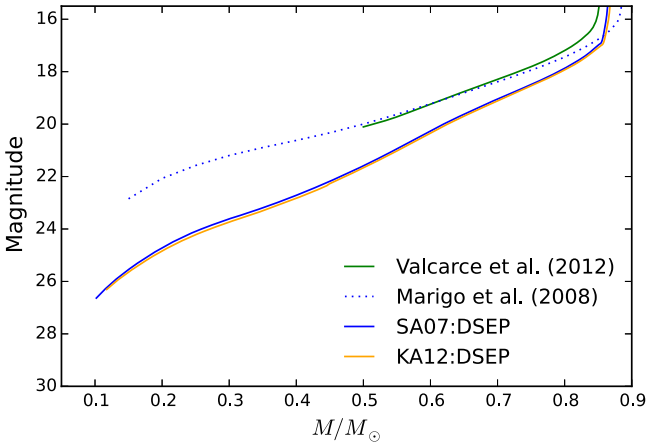

Figure 6. MLR based on the DSEP, PGPUC (Valcarce et al. 2012), and Padova (Marigo et al. 2008; Girardi et al. 2010) models for both the VMC's *Y*-band magnitudes and the *HST* F606W filter. The blue and orange curves are the DSEP MLRs for the *HST* data, while the green curve represents the PGPUC model for the VMC data. The dotted line is the Padova model pertinaing to the VMC data, shown for comparison.

that dynamical mass segregation can indeed happen for both stellar generations in 47 Tuc.

Figure 8 shows $t_{\rm relax}$ as a function of the initial half-mass radius[20] ($r_{\rm h}$) for FG and SG stars under the assumptions that 47 Tuc is dominated by FG stars in the GC formation scenario, where we assumed a typical stellar mass for 47 Tuc of $m_* = 0.72 M_\odot$. We also assumed $M_{\rm SG} = 5 \times 10^5\ M_\odot$ and $M_{\rm FG} = 2.5 \times 10^6\ M_\odot$, based on the following arguments. The observed total mass of 47 Tuc is about $7 \times 10^5\ M_\odot$ (Forbes & Bridges 2010), and we assume that the observed fraction of SG stars in GCs is approximately 70% (since we do not know exactly the current total mass of SG stars in 47 Tuc). The current total mass of SG stars is then approximately $5 \times 10^5\ M_\odot$. Previous theoretical models predict that the FG stars should be 5–10 times more massive than $M_{\rm SG}$, which implies that the initial total mass of the FG stars in the cluster ($M_{\rm FG}$) must be at least $2.5 \times 10^6\ M_\odot$. Consequently, we found that (i) $t_{\rm relax}$ of SG stars is less than 13 Gyr for $r_{\rm h} \leqslant 19.1$ pc. This means that mass segregation of SG stars is possible for 47 Tuc within the observed half-mass radius of 9.6 pc, (ii) $t_{\rm relax}$ of FG stars is less than 13 Gyr for $r_{\rm h} \leqslant 12.3$ pc. This implies that mass segregation can also happen for the initial FG population of 47 Tuc, provided that the initial FG population was as compact as the cluster's present configuration. Even though the above argument is oversimplified in the sense that we have estimated $t_{\rm relax}$ separately for FG and SG stars while in reality the two populations will interact dynamically, this simple estimate has shown that irrespective of the stellar generation, 47 Tuc must be dynamically relaxed at its observed half-mass radius (9.6 pc), a region covered by our *HST* data.

As opposed to the inner region of 47 Tuc, the MF based on our VMC data, which covers the radial range from $r = 500''$ to $r = 1100''$, exhibits an almost constant power-law index: see Figure 7. This observed slight decrease of the α index out to radii of $r \in [500, 600]''$, followed by the absence of any radial trend, provides evidence againsts the importance of mass

[20] The observed half-mass radius of 47 Tuc is $r_{\rm h} \approx 9.6 \pm 0.3$ pc (at the location of KA12's field), based on dynamical modeling (Meylan 1989), which is consistent with $r_{\rm h} = 10$ pc used in the recent simulations of Lane et al. (2012).

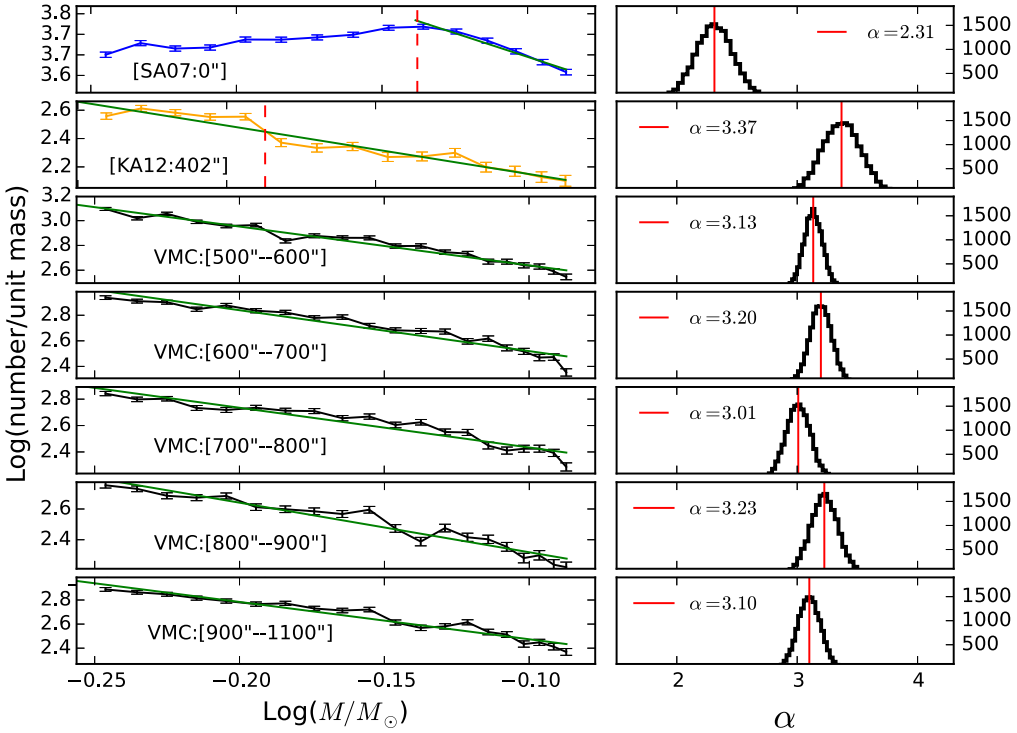

Figure 7. 47 Tuc MFs, obtained by dividing the slope of the MLR by the LFs of Figure 5. Top two panels: the SA07 MF, pertaining to the cluster's central region, shows a decline in stellar numbers for $m_* < 0.72M_\odot$. In contrast, the KA12-based MF in the outer region reveals a deficit for $m_* > 0.65M_\odot$. Bottom five panels: MFs at different radii in the outskirts of 47 Tuc. All annuli exhibit power laws, with no evidence of any deficit or surplus for masses in excess of 0.6 $M_\odot$. We thus fitted all the MFs with the power laws and performed Monte Carlo simulations, shown on the right.

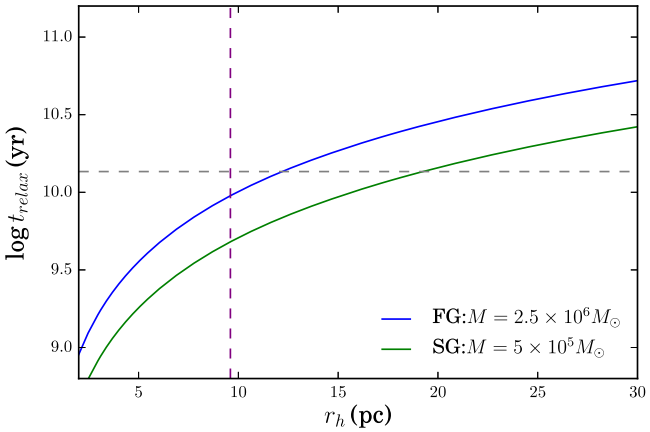

Figure 8. Half-mass relaxation timescale for (blue) first-generation stars and (green) second-generation stars as a function of radius in 47 Tuc. The gray dashed line represents an age of 13 Gyr, which intersects the first-generation prediction at $r = 12.3$ pc and the second-generation curve at $r = 19.1$ pc. The purple dashed line represents the observed half-mass radius at $r = 9.6$ pc.

segregation at these radii, which would have led to a gradual increase of α with increasing radius (to at least 12.3 pc $\equiv 550''$). Therefore, an additional dynamical effect must be contributing to this unchanged α index. This might be due to the effects of tidal stripping, in the sense that shock interactions of 47 Tuc with the Galactic plane's gravitational potential can remove low-mass stars from the cluster's periphery. Lane et al. (2010) found that 47 Tuc exhibits a rise in its local velocity dispersion at large radii; subsequently Küpper et al. (2010) found a similar increase in the cluster's velocity dispersion in their *N*-body simulations, which included the presence of the Galactic tidal field. Küpper et al. (2010) suggested that stars exhibiting abnormal velocities at large radii may be "potential escapers," which is an indication of relaxation-driven evaporation, resulting in the transfer of escaping stars from a cluster to its tidal tails (Fukushige & Heggie 2000). Based on this latter scenario, 47 Tuc is expected to have cold tidal tails at relatively large radii in its outer region (Lane et al. 2012). Therefore, the overall picture that is emerging on the basis of the observed MFs is that mass segregation leads to high-mass stars moving to the cluster core, while ejecting low-mass stars to its periphery. This is where tidal stripping occurs, which removes the low-mass stars from the cluster through gravitational interactions with the Milky Way's tidal field.

This overall picture can be further enriched by the presence of FG and SG stars in 47 Tuc. Milone et al. (2012) found that the fraction of red red giant branch (RGB) stars increases from the cluster's periphery (60%) to its central regions (80%). Li et al. (2014) used VMC data to show that the fraction of RGB and subgiant-branch stars in the core is about 90% and decreases to 10% in the cluster's periphery. We show all MF indices as a function of radius in Figure 9 (top), together with the fraction of FG stars (middle) and its derivative (bottom; smoothed). We note that α peaks for $r \in [380, 500]''$, a region which is indicated by the two red dashed lines. The α distribution then gradually becomes constant. This behavior coincides remarkably well with that of the derivative of the fraction of the FG of stars as a function of radius, which peaks in the same radial range. The derivative of the fraction of FG stars with radius can be intuitively interpreted as the strength of the combined effects of mass segregation and tidal stripping as a function of radius, i.e., the closer to the core of the cluster one looks, the easier it is to observe the effects of mass segregation.

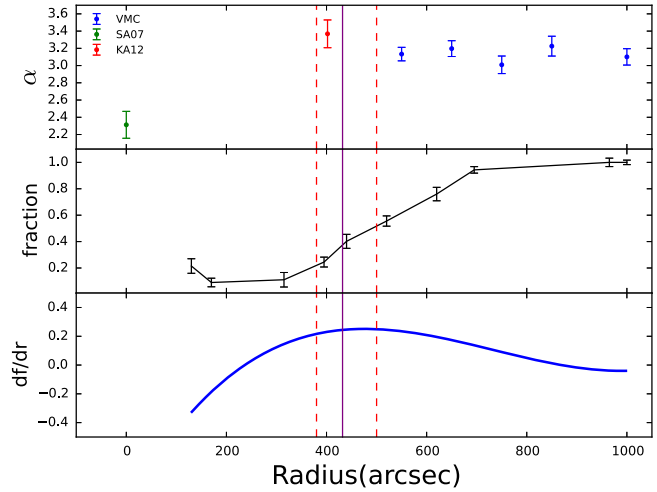

Figure 9. Top: α as a function of radius in 47 Tuc. Middle: fraction of FG stars, obtained by averaging the distributions of RGB and subgiant-branch stars in Li et al. (2014). Bottom: derivative of the fraction of FG stars vs. radius. The purple solid indicates the half-mass radius at about 9.6 pc (430″; we adopted a distance of 4.6 kpc to 47 Tuc) from the center of the cluster.

At radii where mass segregation dominates, one would expect smaller fractions of FG stars to remain; similarly, the effects of tidal stripping start to dominate from radii closer to the cluster's half-mass radius outward. The fraction of FG stars is inversely correlated with the strength of the tidal stripping process.

But why is there also such a peak at radii $r \in [380, 500]''$? We suggest that this may be due to the competing effects of mass segregation on the one hand and tidal stripping on the other. The observed flattening of the MF toward the cluster core is caused by the FG massive stars having undergone mass segregation and, hence, they have migrated to the cluster center. This consequently increased the number of high-mass stars in the central regions (and, equivalently, increased the number of low-mass stars in the periphery). This process can proceed very rapidly in the cluster core, particularly if the core has initial substructure (e.g., Küpper et al. 2011). SG stars will then form spatially more centrally from recycled FG stellar matter. Since the newly formed SG stars are more centrally concentrated, their spatial distribution would be relatively insensitive to the effects of tidal stripping. On the other hand, in the outskirts of the cluster, both FG and SG stars should be stripped tidally by the Milky Way's potential. The stripping efficiency of the two generations is different, with the FG being more efficiently stripped owing to its initially more diffuse configuration. As a consequence, tidal stripping of low-mass FG stars leads to a flatter α index toward larger radii, as indicated by our VMC observations. The observed peak in the α distribution is therefore likely caused by a combination of mass segregation and tidal stripping operating at $r \in [380, 500]''$.

5. CONCLUSIONS

In this paper, we have investigated the LFs and MFs of the low-mass MS stars in 47 Tuc as a function of radius. We have used near-infrared observations, obtained as part of the VMC survey, located at clustercentric radii of 500″–1100″, as well as data from two complementary *HST* data sets, one located in the central region and the other at a distance of 6.′7 from the cluster center. Our key results are as follows.

1. The *HST*-based LFs and MFs suggest that the stellar numbers decline for magnitudes of $18.75 \leqslant \mathrm{F606W} \leqslant 20.9$ in the center of the cluster, corresponding to a mass range of $0.55 < m_*/M_\odot < 0.73$. Contrary to this result, we found that the MF at 6.′7 from the cluster center exhibits a deficit in stars at higher masses, $0.65 < m_*/M_\odot < 0.82$. This is in support of the expectations from mass segregation, i.e., the high-mass stars sink to the center of the cluster and dynamically boost the lower-mass stars to the outer regions.
2. The 47 Tuc LFs and MFs based on the VMC VISTA data all exhibit power-law shapes in the mass range $0.55 < m_*/M_\odot < 0.82$, with slopes remaining almost unchanged. This is likely due to tidal stripping, which is expected to remove the lower-mass FG stars from the outer regions of the cluster.
3. Combining the VMC and *HST* observations, the MF index increases from the inner region outward and reaches a peak at a radius of about 380″–500″; it subsequently decreases and remains constant toward the cluster's periphery. This peak in the α distribution at radii $r \in [380, 500]''$ (close to the half-mass radius) could be due to the combined effects of mass segregation and tidal stripping on the cluster's FG and SG stars.

The analysis in this article is based on observations made with the VISTA telescope at the European Southern Observatory under program ID 179.B-2003. We thank the team responsible for the UK's VISTA Data Flow System for providing calibrated data products, supported by the UK's Science and Technology Facilities Council. We also would like to thank the Globular Cluster Treasury program team (PI: A. Sarajedini) for their guidance on the *HST* completeness table. C.Z. is grateful to the Kavli Institute for Astronomy and Astrophysics for their hospitality and dedicated assistance during the period of this work, and special thanks are due to Yang Huang for his insightful discussions on data reduction. C.Z., C.L., and R.d.G. acknowledge funding support from the National Natural Science Foundation of China (grant 11373010). C.Z., L.C., and C.L. acknowledge financial support from "973 Program" 2014 CB845702 and the Strategic Priority Research Program "The Emergence of Cosmological Structures" of the Chinese Academy of Sciences (CAS; grants XDB09010100 and XDB09000000).

REFERENCES

Anderson, J., & King, I. R. 1996, in ASP Conf. Ser. 92, Formation of the Galactic Halo. Inside and Out, ed. H. L. Morrison & A. Sarajedini (San Francisco, CA: ASP), 257
Anderson, J., Piotto, G., King, I. R., Bedin, L. R., & Guhathakurta, P. 2009, ApJL, 697, L58
Anderson, J., Sarajedini, A., Bedin, L. R., et al. 2008, AJ, 135, 2055
Bekki, K. 2011, MNRAS, 412, 2241
Bochanski, J. J., Hawley, S. L., Covey, K. R., et al. 2010, AJ, 139, 2679
Bonnell, I. A., Larson, R. B., & Zinnecker, H. 2007, Protostars and Planets V, ed. B. Reipurth, D. Jewitt & K. Keil (Tuscon, AZ: Univ. Arizona Press), 149
Cioni, M.-R. L., Clementini, G., Girardi, L., et al. 2011, A&A, 527, A116
de Grijs, R., Gilmore, G. F., Johnson, R. A., & Mackey, A. D. 2002, MNRAS, 331, 245
de Marchi, G., & Paresce, F. 1995, A&A, 304, 211
D'Ercole, A., D'Antona, F., Ventura, P., Vesperini, E., & McMillan, S. L. W. 2010, MNRAS, 407, 854
Dotter, A., Chaboyer, B., Jevremović, D., et al. 2008, ApJS, 178, 89
Forbes, D. A., & Bridges, T. 2010, MNRAS, 404, 1203
Fukushige, T., & Heggie, D. C. 2000, MNRAS, 318, 753

Giersz, M., & Heggie, D. C. 2011, MNRAS, 410, 2698
Girardi, L., Williams, B. F., Gilbert, K. M., et al. 2010, ApJ, 724, 1030
Harris, W. E. 1996, AJ, 112, 1487
Hesser, J. E., Harris, W. E., Vandenberg, D. A., et al. 1987, PASP, 99, 739
Heyl, J., Richer, H. B., Antolini, E., et al. 2015, ApJ, 804, 53
Irwin, M. J., Lewis, J., Hodgkin, S., et al. 2004, Proc. SPIE, 5493, 411
Kalirai, J. S., Anderson, J., Dotter, A., et al. 2013, ApJ, 763, 110
Kalirai, J. S., Richer, H. B., Anderson, J., et al. 2012, AJ, 143, 11
King, I. 1958, AJ, 63, 465
Kroupa, P., Tout, C. A., & Gilmore, G. 1990, MNRAS, 244, 76
Küpper, A. H. W., Kroupa, P., Baumgardt, H., & Heggie, D. C. 2010, MNRAS, 407, 2241
Küpper, A. H. W., Maschberger, T., Kroupa, P., & Baumgardt, H. 2011, MNRAS, 417, 3200
Lane, R. R., Brewer, B. J., Kiss, L. L., et al. 2010, ApJL, 711, L122
Lane, R. R., Küpper, A. H. W., & Heggie, D. C. 2012, MNRAS, 423, 2845
Larson, R. B. 1992, MNRAS, 256, 641
Li, C., de Grijs, R., Deng, L., et al. 2014, ApJ, 790, 35
Marigo, P., Girardi, L., Bressan, A., et al. 2008, A&A, 482, 883
Meylan, G. 1989, A&A, 214, 106
Milone, A. P., Piotto, G., Bedin, L. R., et al. 2012, ApJ, 744, 58
Padoan, P., & Nordlund, Å. 2002, ApJ, 576, 870
Paust, N. E. Q., Reid, I. N., Piotto, G., et al. 2010, AJ, 139, 476
Pietrinferni, A., Cassisi, S., Salaris, M., & Castelli, F. 2006, ApJ, 642, 797
Rubele, S., Girardi, L., Kerber, L., et al. 2015, MNRAS, 449, 639
Rubele, S., Kerber, L., Girardi, L., et al. 2012, A&A, 537, A106
Santiago, B. X., Elson, R. A. W., & Gilmore, G. F. 1996, MNRAS, 281, 1363
Sarajedini, A., Bedin, L. R., Chaboyer, B., et al. 2007, AJ, 133, 1658
Spitzer, L., Jr., & Hart, M. H. 1971, ApJ, 166, 483
Stetson, P. B. 1987, PASP, 99, 191
Valcarce, A. A. R., Catelan, M., & Sweigart, A. V. 2012, A&A, 547, A5